Original Research Article

Positron emission tomography guided dose painting by numbers of lung cancer: Alanine dosimetry in an anthropomorphic phantom

Iosif Papoutsis [a], Ingerid Skjei Knudtsen [b,c,*], Erlend Peter Skaug Sande [b], Bernt Louni Rekstad [b], Michel Öllers [d], Wouter van Elmpt [d], Marius Røthe Arnesen [b], Eirik Malinen [a,b]

[a] *Department of Physics, University of Oslo, P.O. Box 1048 Blindern, N-0316 Oslo, Norway*
[b] *Department of Medical Physics, Oslo University Hospital, P.O. Box 4953 Nydalen, N-0424 Oslo, Norway*
[c] *Department of Circulation and Medical Imaging, Norwegian University of Science and Technology, P.O. Box 8905, N-7491 Trondheim, Norway*
[d] *Department of Radiation Oncology (MAASTRO), GROW – School for Oncology and Developmental Biology, Maastricht University Medical Center, P.O. Box 616, 6200 MD Maastricht, the Netherlands*

ARTICLE INFO

ABSTRACT

Background and purpose: Dose painting by numbers (DPBN) require a high degree of dose modulation to fulfill the image-based voxel wise dose prescription. The aim of this study was to assess the dosimetric accuracy of ^{18}F-fluoro-2-deoxy-glucose positron emission tomography(^{18}F-FDG-PET)-based DPBN in an anthropomorphic lung phantom using alanine dosimetry.
Materials and methods: A linear dose prescription based on ^{18}F-FDG-PET image intensities within the gross tumor volume (GTV) of a lung cancer patient was employed. One DPBN scheme with low dose modulation (Scheme A; minimum/maximum fraction dose to the GTV 2.92/4.26 Gy) and one with a high modulation (Scheme B; 2.81/4.52 Gy) were generated. The plans were transferred to a computed tomograpy (CT) scan of a thorax phantom based on CT images of the patient. Using volumetric modulated arc therapy (VMAT), DPBN was delivered to the phantom with embedded alanine dosimeters. A plan was also delivered to an intentionally misaligned phantom. Absorbed doses at various points in the phantom were measured by alanine dosimetry.
Results: A pointwise comparison between GTV doses from prescription, treatment plan calculation and VMAT delivery showed high correspondence, with a mean and maximum dose difference of <0.1 Gy and 0.3 Gy, respectively. No difference was found in dosimetric accuracy between scheme A and B. The misalignment caused deviations up to 1 Gy between prescription and delivery.
Conclusion: DPBN can be delivered with high accuracy, showing that the treatment may be applied correctly from a dosimetric perspective. Still, misalignment may cause considerable dosimetric erros, indicating the need for patient immobilization and monitoring.

1. Introduction

The concept of biologic image guided radiotherapy (RT) dose delivery – dose painting – was introduced in the early 2000 s [1]. The strategy is to use biologic imaging such as magnetic resonance imaging (MRI) or positron emission tomography (PET) to prescribe a heterogeneous dose delivery to the target volume, based on the assumption that the images reflect the inherent radiosensitivity of the tumour. Two different approaches are commonly applied, dose painting by contours (DPBC) and dose painting by numbers (DPBN). DPBC implies dividing the target volume into two (or more) regions, where each region is prescribed to a different dose. For DPBN, each voxel is prescribed a dose based on a mathematical model connecting voxel intensity and radiosensitivity. While DPBC is relatively straightforward to implement in commercial treatment planning systems (TPS), DPBN relies on in-house add-ons or research versions of the TPS [2–5].

Results of clinical dose painting trials are only now starting to emerge. For prostate cancer, the FLAME trial showed no increase in toxicities and higher biochemical disease-free survival for patients receiving an MR guided boost of the dominant intraprostatic lesion compared to patients receiving conventional RT [6,7]. Similar results have been reported in another prostate dose painting trial, based on ^{18}F-choline PET and MR [8]. In the PET boost trial for non-small cell lung cancer (NSCLC), where one study arm receives a homogenous dose escalation and the other a ^{18}F-fluoro-2-deoxy-glucose (FDG)-PET based simultaneous integrated boost, increased acute and late toxicities have been reported [9,10]. However, the toxicities were within preset constraints and results stratified by study arm are not available yet. For head and neck cancer (HNC), ^{18}F-FDG based adaptive dose painting by numbers (DPBN) has resulted in better 1- and 2-year local control but no significant difference in overall survival compared to intensity-modulated radiotherapy with a homogeneous tumour dose (IMRT) [11]. Previous trials have demonstrated the technical and clinical feasibility of DPBN, but also that heterogeneous dose escalation increases the risk of radiation induced toxicities [12–15]. To minimize the risk of toxicity, it is important to ensure that the prescribed dose distribution can be accurately delivered to the patient.

To our knowledge, few studies have addressed dosimetric accuracy of dose painting. Our groups have previously investigated the accuracy and precision of DPBC [16], where the applied DPBC strategy was equal to that implemented in the PET boost trial for locally advanced lung cancer [10]. Such patients have large primary tumours showing less motion compared to patients with low stage cancer eligible for stereotactic ablative RT [17]. Thus, DPBN may be a feasible approach for these patients as the target is relatively stable. Still, lung tumors are located in a dosimetrically challenging region comprising soft tissue, lung, and bone. This tissue heterogeneity may cause inaccuracies in the dose calculations, especially when applying small beam segments during IMRT or volumetric modutaled arc therapy (VMAT) [18]. This may further lead to errors in the DPBN plan and dose delivery.

For DPBN, with higher demands on the performance and capabilities of the TPS and the linear accelerator, no dosimetry studies have so far been published. This is likely due to the fact that a comprehensive procedure is required, starting with the voxel-by-voxel dose prescription in the tumour followed by treatment plan optimization and dose calculation and finally the dose delivery. The aim of the current work was to perform an evaluation of the dosimetric accuracy of clinically relevant DPBN plans step-by-step in a static, anthropomorphic phantom based on PET/computed tomography (CT) images of a lung cancer patient. We employed alanine dosimetry [19] for a pointwise assessment of the DPBN delivery in the phantom, as alanine is a small, passive dosimeter (with minimal perturbation of the phantom) showing a highly linear dose response.

2. Materials and methods

2.1. Patient and thorax phantom

A static, anthropomorphic true-size thorax phantom was constructed based on ^{18}F-FDG-PET/CT images of a male NSCLC patient with a gross tumour volume (GTV) of 184 cm^3. The phantom contained cavities for alanine dosimeters in and around the GTV. Details of the ^{18}F-FDG-PET/CT image acquisition parameters and phantom construction can be found in an earlier publication [16]. The patient was part of the PET boost clinical trial cohort and signed informed consent before registering in the study [10]

2.2. DPBN prescription, planning and delivery

The gross tumour volume (GTV), planning target volume (PTV; GTV + 5 mm) and organs at risk (OAR; lungs, spinal cord and oesophagus) were delineated on the patient's ^{18}F-FDG-PET/CT images in the TPS

(Eclipse, version 10.0, Varian Medical Systems, Inc., Palo Alto, USA). The GTV structure and PET images were used for calculating DPBN prescriptions in an in-house developed program [5] using IDL (version 8.2, Interactive Data Language, Harris Geospatial Solutions, Florida, USA). All reported doses are per fraction, following the PET boost trial design employing 24 fractions with a mean fraction dose to the PTV of typically 3 Gy [10]. A linear relationship between prescribed voxel dose D_v to the GTV and PET image voxel intensity I_v was applied [20]:

$$D_v = D_{low} + \frac{I_v - I_{low}}{I_{high} - I_{low}}\left(D_{high} - D_{low}\right) \tag{1}$$

I_{high} and I_{low} were defined from the 95th and 5th percentile of the ^{18}F-FDG uptake in the tumour. Using eq. (1), different prescription schemes can be made by altering the minimum and maximum prescribed dose D_{low} and D_{high}, respectively. We generated two schemes (A and B) where the D_{low} and D_{high} varied but were the mean tumour dose D_{mean} was identical and set to 3.2 Gy. In scheme A, D_{low} was set to 2.92 Gy and D_{high} to 4.26 Gy. In scheme B, D_{low} was set to 2.81 Gy and D_{max} to 4.52 Gy. In the central axial plane of the GTV, this gave a maximum dose gradient of about 0.046 and 0.050 Gy/mm for scheme A and B, respectively. Thus, scheme B required a higher degree of dose modulation across the GTV and may be more challenging to plan and deliver accurately.

For both schemes, the dose assigned to the PTV was equal to the respective D_{low}. Additionally, an inverse 3D dose prescription matrix was calculated by subtracting the original DPBN matrix from D_{high} for each scheme. The inverse dose prescription matrices were transferred to the TPS and used as basis for optimizing two 6 MV DPBN Volumetric Modulated Arc Therapy (VMAT) plans (see [5] for details on this methodology). Dose constraints for the OARs were included in the optimization. Resulting dose distributions were calculated by the Analytical Anisotropic Algorithm (AAA, version 10.0.28), thus resulting in two DPBN treatment plans A and B in the patient CT-basis. All structures and optimized plans were then transferred to the phantom CT basis where the dose distributions were re-calculated. The experimental set-up of the study is schematized in Fig. S1 in supplementary materials.

In the following, D_{pres} is the dose prescription resulting from the linear conversion of the ^{18}F-FDG image intensities within the GTV (Eq. (1)), D_{plan} is the calculated dose in the treatment planning system, and D_{del} is the delivered dose measured by alanine dosimetry, as described in the last paragraph of this section. As the patient plan had to be recalculated in the phantom, prescribed GTV doses in the phantom were estimated by scaling the patient-based prescription by the ratio of the planned calculated doses in the phantom and patient voxel by voxel.

Irradiation of the phantom (and dosimeters) was performed at a Varian Trilogy linear accelerator (Varian Medical Systems) with a 120 leaf Millennium multi leaf collimator. Both scheme A and B was delivered to the phantom. The phantom position was verified by cone beam CT prior to irradiation, resulting in a geometric accuracy of about 1 mm. An additional irradiation was performed using scheme A, but where the phantom was repositioned with a shift of 5 mm in the x-, y- and z-directions (scheme A_shift). This corresponded to a vector shift of 8.7 mm. For each of the three irradiations, four fractions were delivered to the phantom in order to achieve dose levels suitable for alanine dosimetry.

For dose measurements, Electron Paramagnetic Resonance (EPR) dosimetry was employed. More details can be found in a previous publication [16]. For each of the measurement series, a calibration curve was constructed based on irradiation of 3x5 dosimeters to 2, 6, 10, 14 and 18 Gy in a water tank. This range of doses was selected to cover the absorbed doses of the dosimeters in the target volumes and nearest organs at risk (for four fractions of irradiation). For a given alanine dosimeter irradiated in the lung phantom, the dose was thus estimated from the corresponding calibration curve. The absolute dosimetric uncertainty was estimated to 0.03 Gy per fraction, based on residual analysis of these curves (data not shown). The calibration curves are shown in Fig. S2 in Supplementary materials. For the phantom

measurements, the number of measurement points within the GTV was 38 for scheme A and 41 for scheme B and scheme A_shift. For normal tissues (typically lung) the number of measurement points was 35, 20 and 16, respectively.

To further assess the sensitivity of the plan to displacement, we simulated a shift of the phantom in the treatment planning system by moving the isocentre of the treatment plan ± 2.5 mm (magnitude of shift 4.3 mm) and ± 5.0 mm (magnitude of shift 8.7 mm) in all directions and recalculating the dose for scheme A.

2.3. Evaluation and analysis

As the dosimeters were visible in the CT images of the phantom, point-to-point comparison of D_{pres}, D_{plan}, and D_{del} could be performed. Mean, standard deviation and range were calculated for all plans A, B and A_shift for the PTV and normal tissue. Statistical analyses were performed in Stata (vers 16.1, StataCorp LLC, USA). For each plan, the differences between D_{pres}, D_{plan} and D_{del} were evaluated by the Wilcoxon matched-pairs signed-rank test, applying the Bonferroni correction to adjust for multiple testing. The mean differences of D_{pres}-D_{plan}, D_{pres}-D_{del}, and D_{plan}-D_{del} for scheme A versus scheme B were compared by an unpaired two-sample *t*-test, with a level of p < 0.05 (two-sided) considered significant. Furthermore, to evaluate the overall deviations between prescribed, planned and delivered doses, the quality factor (QF) [2] was calculated

$$QF = \frac{1}{N}\sum_i |Q_i - 1| \qquad (2)$$

where $Q_i = D_i^{p'}/D_i^{p}$. The quality index (Q_i) was determined for all point doses i, as the ratio D_{plan}/D_{pres}, D_{del}/D_{pres} or D_{del}/D_{plan}. N is the number of measurements within a volume (GTV or PTV). To further assess the sensitivity of QF to changes in displacement in more systematic manner, we simulated a shift of the phantom in the treatment planning system by moving the isocentre of the treatment plan ± 2.5 (magnitude of shift 4.3 mm) and ± 5.0 mm (magnitude of shift 8.7 mm) in all directions and recalculating the dose. QF was then calculated for the prescribed dose relative to the calculated plan dose after the simulated shift.

3. Results

3.1. Patient and phantom treatment plans

For the optimized patient plan, the calculated dose distribution for scheme A) had minimum, mean and maximum dose of 2.81, 3.40 and 4.40 Gy to the GTV, respectively. For scheme B), we found a minimum, mean and maximum dose of 2.64, 3.48 and 4.84 Gy, respectively. For both schemes, the mean dose to the PTV was 3.20 Gy. Doses to the OARs were within Oslo University Hospital's tolerance for both plans. For the phantom, the recalculated doses were in general lower than for the patient, and the mean dose to the GTV was 0.06 Gy (<2%) lower for scheme A. The optimized calculated plans for both patient and phantom are summarized in Table 1. Fig. 1 shows the treatment plan for both patient and phantom through a central slice of the tumour (see Fig. S3 in the Supplementary materials for CT images of the three central slices of the phantom with dosimeter positions marked).

3.2. Pointwise comparison of prescribed, calculated and delivered doses

Mean prescribed, planned and delivered fraction doses for the measurement points within the PTV were (3.47, 3.42, 3.39) Gy for scheme A and (3.56, 3.54, 3.51) Gy for scheme B. For scheme A_shift, the mean delivered dose was 3.38 Gy. Table 2 presents the mean difference, standard deviation, range for D_{pres}-D_{plan}, D_{pres}-D_{del}, and D_{plan}-D_{del} within the PTV. The largest deviations were found between the prescribed and the delivered doses (Fig. 2). These findings are further reflected in QFs

Table 1

Summary of optimized plans for patient and phantom. Doses are given per fraction.

Structure	Scheme A (D_{min} = 2.92 Gy)					
	Patient			Phantom		
	Mean dose [Gy]	Min dose [Gy]	Max dose [Gy]	Mean dose [Gy]	Min dose [Gy]	Max dose [Gy]
GTV	3.40	2.81	4.40	3.30	2.69	4.26
PTV	3.20	2.52	4.40	3.11	2.41	4.26
Lungs	0.48	0.00	3.14	0.75	0.06	3.35
Spinal cord	0.10	0.00	1.53	0.59	0.03	1.49
Esophagus	1.19	0.26	2.24	1.18	0.31	2.19

Structure	Scheme B (D_{min} = 2.81 Gy)					
	Patient			Phantom		
	Mean dose [Gy]	Min dose [Gy]	Max dose [Gy]	Mean dose [Gy]	Min dose [Gy]	Max dose [Gy]
GTV	3.48	2.64	4.84	3.36	2.59	4.70
PTV	3.20	2.33	4.84	3.11	2.24	4.70
Lungs	0.48	0.00	3.10	0.74	0.06	3.51
Spinal cord	0.11	0.00	1.70	0.61	0.03	1.65
Esophagus	1.20	0.28	2.23	1.18	0.31	2.13

≤ 2.0 % for D_{pres} *vs* D_{plan} and D_{plan} *vs* D_{del}, while the QFs of D_{pres} *vs* D_{del} were 3.1 % and 2.8 % for scheme A and B, respectively. For scheme A, differences between prescribed, planned and delivered doses were statistically significant, while only D_{pres} and D_{del} were significantly different for scheme B. Although the differences were larger for scheme A than scheme B, this was not statistically significant (p = 0.33, p = 0.15, p = 0.18, respectively). Linear regression indicated no significant trend in the dose difference with increasing prescription dose (p greater than 0.05). By shifting the phantom on the treatment couch prior to irradiation (scheme A_shift), single point deviations between D_{del} and D_{pres} of more than 1 Gy was observed inside the PTV (Fig. 2). The QFs of D_{pres} /D_{del} and D_{plan}/D_{del} for A$_{shift}$ were 7.9 and 7.7 %, respectively .

For normal tissues outside the PTV, the mean difference between D_{plan} and D_{del} was small for all plans (up to 0.03 Gy), and of the same magnitude as for the PTV. However, the maximum observed differences were 0.16 Gy/13% (A), 0.33 Gy/25 % (B) and 0.52 Gy/34% (A_shift) (Fig. 3 and Table 3).

3.3. Simulated shift in the treatment planning system

For the simulated shifts of the phantom in the TPS, QFs were calculated for the prescribed dose versus the calculated plan dose. For scheme A, the mean QFs were 4.5 %/4.0 % for shifts of ±2.5 mm and 8.5%/8.5% for shifts of ±5.0 mm. Thus, the QF resulting from moving the phantom 5 mm in all directions is lower (7.9%), but on the same level as the simulated shift. Correspondingly, for scheme B the mean QFs were 8.5 %/5.5 % for shift of ±2.5 mm and 11.0%/12.0% for shifts of ±5.0 mm.

4. Discussion

In the present work, an anthropomorphic lung phantom was applied to facilitate a point-by-point dosimetric comparison of prescribed, planned and delivered doses for DPBN. Differences between prescribed and planned doses, assessed by the QF, were small (2 % or less). Differences between planned and delivered doses were on the same level. The plan with the highest dose gradient (scheme B) performed on the same level as the plan with a more moderate dose escalation (scheme A), both with regards to comparing prescription/planning and planning/
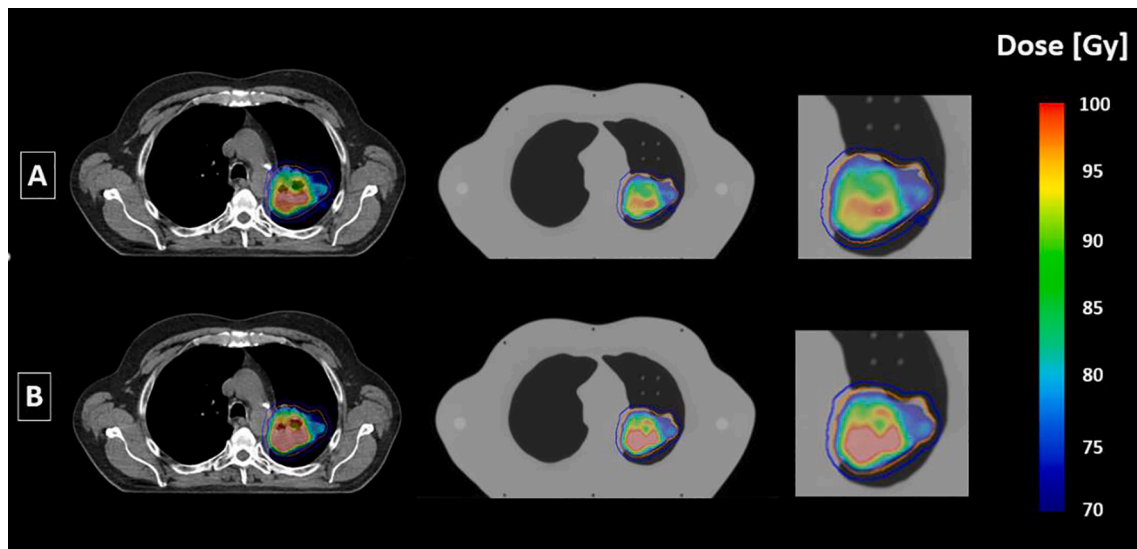
Fig. 1. Optimized treatment plans for patient (left) and phantom (middle and right) for scheme A (above) and scheme B (below). Orange line: GTV, blue line: PTV. Doses are shown corresponding to the whole treatment plans of 24 fractions.

Table 2
Mean difference, standard deviation, range and quality factors for prescribed/planned, prescribed/delivered and planned/delivered doses to the PTV for scheme A, B and A_shift. Values reported are per fraction. * denote a significant p-value.

		Mean difference [Gy]	Std dev [Gy]	Range [Gy]	p-value	QF [%]
Scheme A (n = 38)	D_{pres}-D_{plan}	0.04	0.07	(−0.11,0.18)	0.04*	2.0
	D_{pres}-D_{del}	0.09	0.10	(−0.16, 0.31)	0.00*	3.1
	D_{plan}-D_{del}	0.05	0.05	(−0.10, 0.16)	0.00*	1.7
Scheme B (n = 41)	D_{pres}-D_{plan}	0.02	0.09	(−0.13, 0.26)	0.32	1.7
	D_{pres}-D_{del}	0.06	0.10	(−0.33, 0.30)	0.03*	2.8
	D_{plan}-D_{del}	0.03	0.08	(−0.20, 0.19)	0.07	1.9
Scheme A_shift (n = 41)	D_{pres}-D_{plan}	0.04	0.07	(−0.11, 0.18)	–	2.0
	D_{pres}-D_{del}	0.08	0.40	(−0.84, 1.08)	–	7.9
	D_{plan}-D_{del}	0.04	0.40	(−0.98, 0.96)	–	7.7

delivery. Thus, our study demonstrates that DPBN can be delivered to a static but heterogeneous phantom with high dosimetric accuracy.

In a clinical setting, the accuracy of radiotherapy is hampered by several factors, including patient positioning, inter- and intra- fractional motion and tumour shrinkage. DP radiotherapy plans are even more vulnerable to such effects. Robust optimization strategies, as opposed to target volume based, has been proposed to deal with these issues [21–23]. Also, robust optimization has been introduced for dose painting [24]. Still, target volume based optimization is currently the standard approach in photon based DP radiotherapy planning [22].

Alanine dosimetry is well-established and shows a linear dose response at dose levels employed in radiotherapy, and no dependence on dose rate or fractionation [19]. In our previous study, evaluating DPBC in the same phantom, we estimated the uncertainties of alanine dosimetry in a similar set-up to be below 2.5 %. With a radius of 2.5 mm, the dosimeters are relatively large but comparable to the size of PET voxels, which is an appropriate scale of measurement for dose painting based on PET. Other studies applying alanine dosimetry in a clinical setting have reported differences between planned and delivered doses of 1.5–3.5 % (prostate, in vivo) [25] and within 3 % for whole body irradiation in a humanoid phantom [26]. We observe that the mean difference of planned versus delivered dose is 1.4 % of the mean dose to the tumour for scheme A and 0.7 % for scheme B, although the heterogeneous dose plans applied in the present study should be more challenging than in the other studies, which were aiming at homogenous dose distributions within the target volumes.

The linear PET voxel intensity – dose prescription model applied in the present work correspond to the strategy introduced and applied in several studies by the group in Ghent [11,12,14,27]. There are, however, few studies assessing the actual delivery of dose painted radiotherapy in a clinically relevant setting. In our previous DPBC phantom study [16], the QF (not reported previously) of prescribed versus planned dose was 4.0 %, twice as high as for DPBN in the present work. This reflects the limitations of (two-level) DPBC where the dose, according to the prescription, is escalated in one large step from one voxel to the other. The DPBC QF for planned versus delivered dose was however, 2.2% - on the same level we achieve for DPBN. The challenge of the large dose gradients demanded for two-level DPBC is also illustrated in an early NSCLC planning study by Meijer et al. [3], who calculated QFs separately for the high and low dose part of the GTV. QFs of the low dose part of the GTV ranged from 10 to more than 60 %. In the same study, for DPBN, QFs of the GTV were in no cases higher than 8.8%. For DPBN of HNC, on the other hand, Vanderstraeten et al. has reported an average QF of $1.6 \pm 0.1\%$ (95% CI) for a by-fraction escalation from 2.16 to 2.50 Gy and $3.1 \pm 0.4\%$ for escalation from 2.16 to 3.00 Gy [20]. Arnesen et al. implemented DPBN on three patient cases and reported QFs of 1.8 (HN), 2.0 (lung) and 2.6% (cervix). These discrepancies illustrate that several factors contribute to the overall performance, both patient related (tumour site and its proximity to OARs) and treatment plan related (image derived thresholds for dose prescription, margins, optimization criteria). Moreover, protons may perform better for dose painting, demonstrated on two HNC cases by Barragán et al., where QFs of prescribed *vs* planned doses were 0.94 and 1.03% [28].

For both scheme A and B, we observed some pointwise large deviations between prescribed and delivered doses to the PTV. For scheme B, the delivered dose was in one point 0.3 Gy larger than the prescribed dose, and 0.3 Gy lower in another, which sums up to ± 7.3 Gy over 24
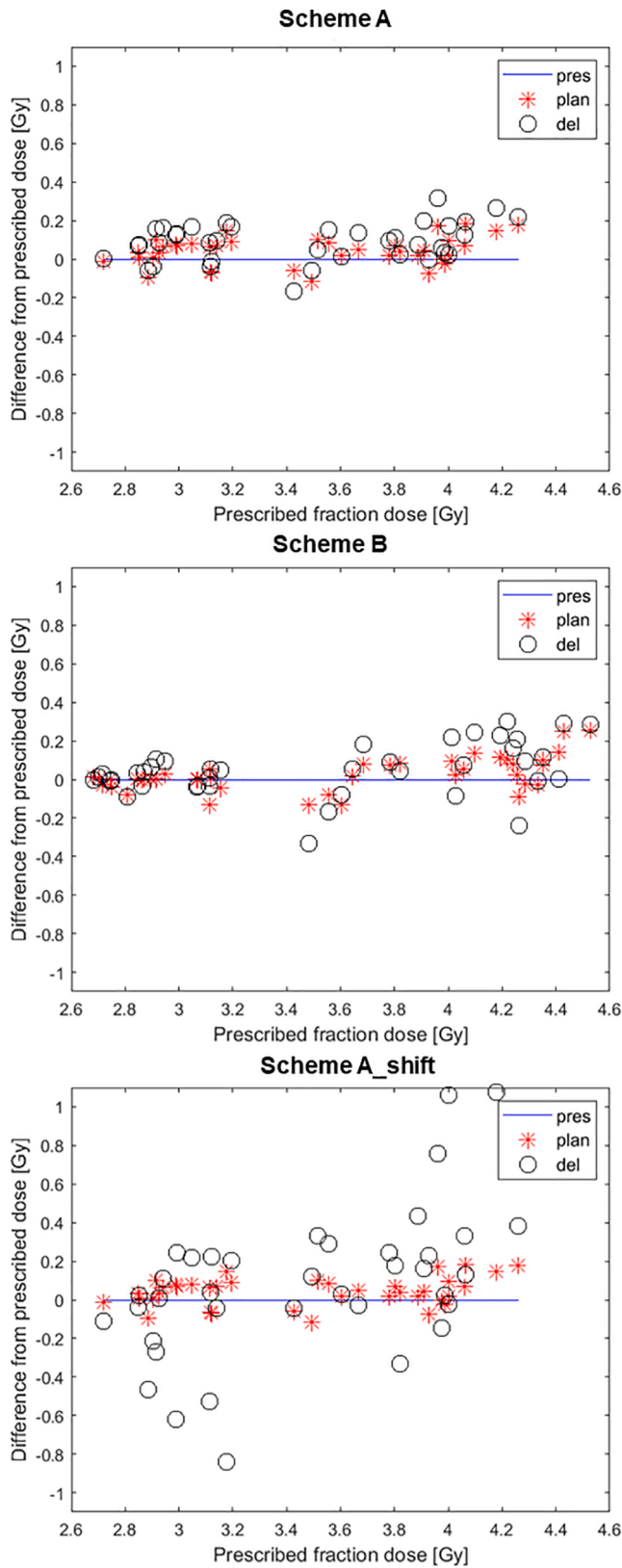
Fig. 2. Difference of the treatment plan dose calculation (*) and delivered (o) doses per fraction to the GTV (phantom), compared to prescription. Top: Scheme A. Middle: Scheme B. Below: Scheme A_shift, where the phantom has been moved 5 mm in the x-, y- and z-directions before irradiation.
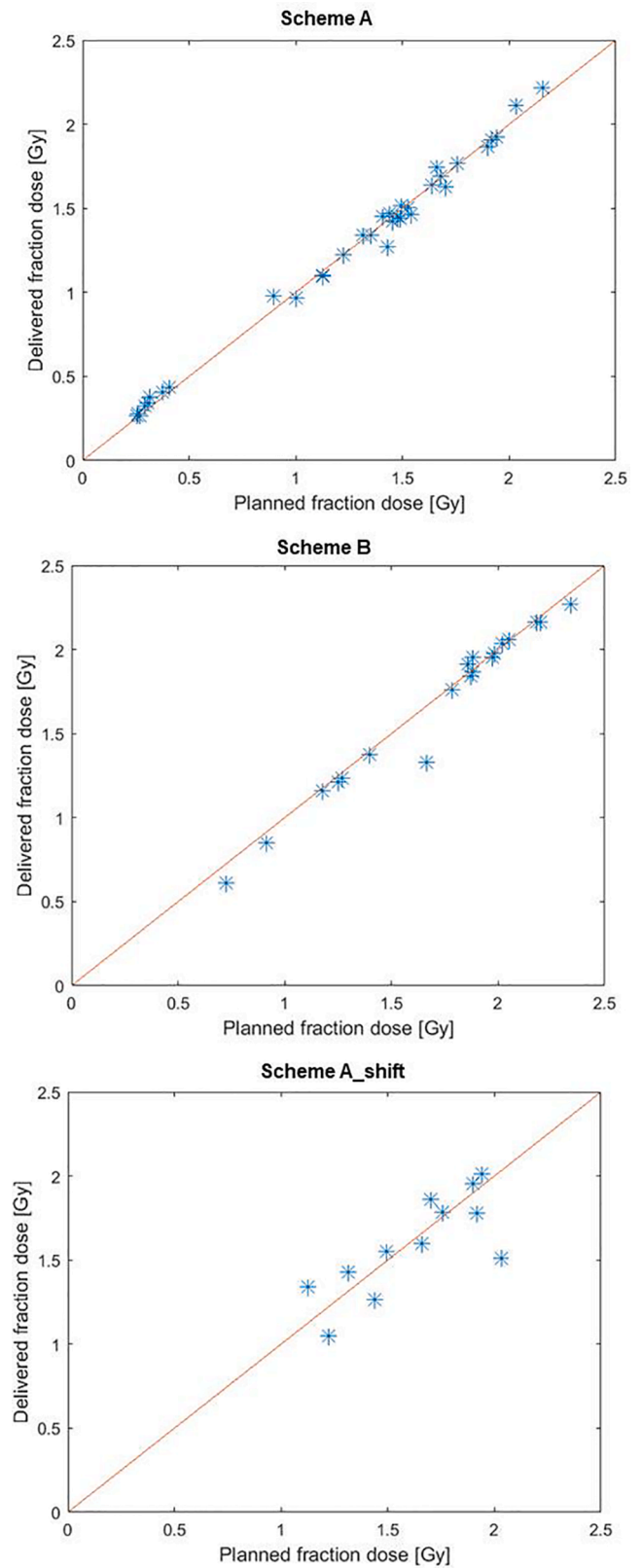
Fig. 3. Planned versus delivered doses to normal tissue (phantom) per fraction. Top: Scheme A. Middle: Scheme B, Below: Scheme A_shift; the phantom has been moved 5 mm in the x-, y- and z-directions before irradiation.

Table 3
Mean difference, standard deviation, and range for planned/delivered doses to normal tissue for Scheme A, B and A_shift. Values reported are per fraction.

		Mean difference [Gy]	Std dev [Gy]	Range [Gy]
Scheme A (n = 35)	D_{plan}-D_{del}	0.00	0.05	(−0.08, 0.16)
Scheme B (n = 20)	D_{plan}-D_{del}	0.03	0.08	(−0.09, 0.33)
Scheme A_shift (n = 16)	D_{plan}-D_{del}	0.02	0.19	(−0.20, 0.50)

fractions. These deviations are, naturally, smaller for the planned versus delivered dose, but could still be clinically significant; over and under-dosage of 0.2 Gy per fraction was observed for scheme B. However, the points of largest deviations were almost exclusively located in the high dose area (>3 Gy). For the normal tissue the mean deviations between planned and prescribed doses were small.

Dose painting plans are vulnerable to displacements and positional errors, demonstrated by large QFs for scheme A_shift and the simulated plans with isocenter shifts. For scheme A_shift, multiple deviations (planned – measured) in the range 0.5–1 Gy are observed within the PTV. The maximum observed overdosage to the normal tissue (0.2 Gy) would sum up to almost 5 Gy extra dose for all fractions. It is unlikely that a patient will undergo treatment with a consistent error in positioning through all fractions, but this finding still illustrates the sensitivity of DPBN to errors. Also, it could be argued that a positioning error of 5 mm in all directions is larger than should be expected by today's treatment standards. However, smaller isocenter shifts (1–2 mm in every direction) have also been found to severely degrade the quality of DPBN treatment plans [29].

Tumour motion during imaging and irradiation will contribute to uncertainties but have not been considered in the present work. The degree of tumour motion depends on several factors [30–32], but one should expect that larger, more advanced tumours suitable for dose painting are less affected than smaller tumours. Larger tumour displacements will lead to larger dose discrepancies, although the summed dose deviation due to respiratory motion after many treatment fractions might not be clinically relevant [33]. Respiratory gated treatment might be preferable in terms of preserving the sharp dose gradients seen in the TPS. Non-gated treatment will inevitably blur the planned dose distribution to some extent. If the PET images acquired for dose prescription are acquired without compensation for motion, they will still reflect the time-averaged intensity of each voxel and might thus be suitable as templates for radiotherapy. Thomas et al. [34] studied the effect of PET motion compensation on the quality of 7 level DPBC plans in a small cohort and found no significant differences in DPBN plan quality. In fact, the choice of segmentation method to define the DPBN boost regions had a greater impact on DPBN plan quality than use of motion compensation [34]. This sensitivity of DPBN plan quality to segmentation method has also been demonstrated previously [35].

In conclusion, we have shown that DPBN can be delivered with high dosimetric accuracy to an anthropomorphic lung phantom. Still, positioning errors and changes in patient anatomy can lead to large deviations and potentially sub-optimal doses to the patient.

Declaration of Competing Interest

The authors declare that they have no known competing financial interests or personal relationships that could have appeared to influence the work reported in this paper.

Acknowledgements

Appendix A. Supplementary data

Supplementary data to this article can be found online at https://doi.org/10.1016/j.phro.2022.02.013.

References

[1] Ling CC, Humm J, Larson S, Amols H, Fuks Z, Leibel S, et al. Towards multidimensional radiotherapy (MD-CRT): biological imaging and biological conformality. Int J Radiat Oncol Biol Phys 2000;47:551–60. https://doi.org/10.1016/s0360-3016(00)00467-3.

[2] Vanderstraeten B, De Gersem W, Duthoy W, De Neve W, Thierens H. Implementation of biologically conformal radiation therapy (BCRT) in an algorithmic segmentation-based inverse planning approach. Phys Med Biol 2006;51:N277–86. https://doi.org/10.1088/0031-9155/51/16/N02.

[3] Meijer G, Steenhuijsen J, Bal M, De Jaeger K, Schuring D, Theuws J. Dose painting by contours versus dose painting by numbers for stage II/III lung cancer: practical implications of using a broad or sharp brush. Radiother Oncol 2011;100:396–401. https://doi.org/10.1016/j.radonc.2011.08.048.

[4] Thorwarth D, Eschmann SM, Paulsen F, Alber M. Hypoxia dose painting by numbers: a planning study. Int J Radiat Oncol Biol Phys 2007;68:291–300. https://doi.org/10.1016/j.ijrobp.2006.11.061.

[5] Arnesen MR, Knudtsen IS, Rekstad BL, Eilertsen K, Dale E, Bruheim K, et al. Dose painting by numbers in a standard treatment planning system using inverted dose prescription maps. Acta Oncol 2015;54:1607–13. https://doi.org/10.3109/0284186X.2015.1061690.

[6] Monninkhof EM, van Loon JWL, van Vulpen M, Kerkmeijer LGW, Pos FJ, Haustermans K, et al. Standard whole prostate gland radiotherapy with and without lesion boost in prostate cancer: Toxicity in the FLAME randomized controlled trial. Radiother Oncol 2018;127:74–80. https://doi.org/10.1016/j.radonc.2017.12.022.

[7] Kerkmeijer LGW, Groen VH, Pos FJ, Haustermans K, Monninkhof EM, Smeenk RJ, et al. Focal boost to the intraprostatic tumor in external beam radiotherapy for patients with localized prostate cancer: results from the FLAME randomized phase III Trial. J Clin Oncol 2021;39:787–96. https://doi.org/10.1200/JCO.20.02873.

[8] Syndikus I, Chan JKC, Rowntree T, Howard L, Staffurth J. Hypofractionated dose painting IMRT using 20 fractions for intermediate to high-risk localized prostate cancer: two-year outcome data (BIOPROP20, NCT02125175). J Clin Oncol 2019; (37).

[9] van Diessen J, De Ruysscher D, Sonke JJ, Damen E, Sikorska K, Reymen B, et al. The acute and late toxicity results of a randomized phase II dose-escalation trial in non-small cell lung cancer (PET-boost trial). Radiother Oncol 2019;131:166–73. https://doi.org/10.1016/j.radonc.2018.09.019.

[10] van Elmpt W, De Ruysscher D, van der Salm A, Lakeman A, van der Stoep J, Emans D, et al. The PET-boost randomised phase II dose-escalation trial in non-small cell lung cancer. Radiother Oncol 2012;104:67–71. https://doi.org/10.1016/j.radonc.2012.03.005.

[11] Duprez F, Daisne JF, Berwouts D, De Gersem W, Goethals I, Olteanu AL, et al. Randomized phase 2 trial of adaptive dose painting vs standard IMRT for head and neck cancer. Radiother Oncol 2019;133:S259–60. https://doi.org/10.1016/S0167-8140(19)30924-7.

[12] Berwouts D, Olteanu LA, Duprez F, Vercauteren T, De Gersem W, De Neve W, et al. Three-phase adaptive dose-painting-by-numbers for head-and-neck cancer: initial results of the phase I clinical trial. Radiother Oncol 2013;107:310–6. https://doi.org/10.1016/j.radonc.2013.04.002.

[13] Duprez F, De Neve W, De Gersem W, Coghe M, Madani I. Adaptive dose painting by numbers for head-and-neck cancer. Int J Radiat Oncol Biol Phys 2011;80:1045–55. https://doi.org/10.1016/j.ijrobp.2010.03.028.

[14] Madani I, Duprez F, Boterberg T, Van de Wiele C, Bonte K, Deron P, et al. Maximum tolerated dose in a phase I trial on adaptive dose painting by numbers for head and neck cancer. Radiother Oncol 2011;101:351–5. https://doi.org/10.1016/j.radonc.2011.06.020.

[15] Madani I, Duthoy W, Derie C, De Gersem W, Boterberg T, Saerens M, et al. Positron emission tomography-guided, focal-dose escalation using intensity-modulated radiotherapy for head and neck cancer. Int J Radiat Oncol Biol Phys 2007;68:126–35. https://doi.org/10.1016/j.ijrobp.2006.12.070.

[16] Knudtsen IS, Svestad JG, Skaug Sande EP, Rekstad BL, Rodal J, van Elmpt W, et al. Validation of dose painting of lung tumours using alanine/EPR dosimetry. Phys Med Biol 2016;61:2243–54. https://doi.org/10.1088/0031-9155/61/6/2243.

[17] Yu ZH, Lin SH, Balter P, Zhang LF, Dong L. A comparison of tumor motion characteristics between early stage and locally advanced stage lung cancers. Radiother Oncol 2012;104:33–8. https://doi.org/10.1016/j.radonc.2012.04.010.

[18] Zhao Y, Qi G, Yin G, Wang X, Wang P, Li J, et al. A clinical study of lung cancer dose calculation accuracy with Monte Carlo simulation. Radiat Oncol 2014;9. https://doi.org/10.1186/s13014-014-0287-2.

[19] Malinen E. EPR Dosimetry in Clinical Applications. In: Lund A, Shiotani M, editors. Applications of EPR in Radiation Research: Springer International Publishing; 2014. p. 509-38. https://doi.org/10.1007/978-3-319-09216-4_14.

[20] Vanderstraeten B, Duthoy W, De Gersem W, De Neve W, Thierens H. [18F]fluoro-deoxy-glucose positron emission tomography ([18F]FDG-PET) voxel intensity-

based intensity-modulated radiation therapy (IMRT) for head and neck cancer. Radiother Oncol 2006;79:249–58. https://doi.org/10.1016/j.radonc.2006.03.003.

[21] Korevaar EW, Habraken SJM, Scandurra D, Kierkels RGJ, Unipan M, Eenink MGC, et al. Practical robustness evaluation in radiotherapy – A photon and proton-proof alternative to PTV-based plan evaluation. Radiother Oncol 2019;141:267–74. https://doi.org/10.1016/j.radonc.2019.08.005.

[22] Outaggarts Z, Wegener D, Berger B, Zips D, Paulsen F, Bleif M, et al. Target miss using PTV-based IMRT compared to robust optimization via coverage probability concept in prostate cancer. Acta Oncol 2020;59:911–7. https://doi.org/10.1080/0284186X.2020.1760349.

[23] Gronlund E, Almhagen E, Johansson S, Traneus E, Ahnesjo A. Robust maximization of tumor control probability for radicality constrained radiotherapy dose painting by numbers of head and neck cancer. Phys Imaging Radiat Oncol 2019;12:56–62. https://doi.org/10.1016/j.phro.2019.11.004.

[24] Petit SF, Breedveld S, Unkelbach J, den Hertog D, Balvert M. Robust dose-painting-by-numbers vs. nonselective dose escalation for non-small cell lung cancer patients. Med Phys 2021;48:3096–108. https://doi.org/10.1002/mp.14840.

[25] Wagner D, Anton M, Vorwerk H, Gsanger T, Christiansen H, Poppe B, et al. In vivo alanine/electron spin resonance (ESR) dosimetry in radiotherapy of prostate cancer: a feasibility study. Radiother Oncol 2008;88:140–7. https://doi.org/10.1016/j.radonc.2008.03.017.

[26] Schaeken B, Lelie S, Meijnders P, Van den Weyngaert D, Janssens H, Verellen D. Alanine/EPR dosimetry applied to the verification of a total body irradiation protocol and treatment planning dose calculation using a humanoid phantom. Med Phys 2010;37:6292–9. https://doi.org/10.1118/1.3496355.

[27] Berwouts D, Madani I, Duprez F, Olteanu AL, Vercauteren T, Boterberg T, et al. Long-term outcome of (18) F-fluorodeoxyglucose-positron emission tomography-guided dose painting for head and neck cancer: Matched case-control study. Head Neck 2017;39:2264–75. https://doi.org/10.1002/hed.24892.

[28] Barragan AM, Differding S, Janssens G, Lee JA, Sterpin E. Feasibility and robustness of dose painting by numbers in proton therapy with contour-driven plan optimization. Med Phys 2015;42:2006–17. https://doi.org/10.1118/1.4915082.

[29] Korreman SS, Ulrich S, Bowen S, Deveau M, Bentzen SM, Jeraj R. Feasibility of dose painting using volumetric modulated arc optimization and delivery. Acta Oncol 2010;49:964–71. https://doi.org/10.3109/0284186X.2010.498440.

[30] Keall PJ, Mageras GS, Balter JM, Emery RS, Forster KM, Jiang SB, et al. The management of respiratory motion in radiation oncology report of AAPM Task Group 76. Med Phys 2006;33:3874–900. https://doi.org/10.1118/1.2349696.

[31] Korreman SS. Image-guided radiotherapy and motion management in lung cancer. Br J Radiol 2015;88. https://doi.org/10.1259/bjr.20150100.

[32] Korreman SS. Motion in radiotherapy: photon therapy. Phys Med Biol 2012;57: R161–91. https://doi.org/10.1088/0031-9155/57/23/R161.

[33] Sande EPS, Acosta Roa AM, Hellebust TP. Dose deviations induced by respiratory motion for radiotherapy of lung tumors: impact of CT reconstruction, plan complexity, and fraction size. J Appl Clin Med Phys 2020;21:68–79. https://doi.org/10.1002/acm2.12847.

[34] Thomas HM, Kinahan PE, Samuel JJE, Bowen SR. Impact of tumour motion compensation and delineation methods on FDG PET-based dose painting plan quality for NSCLC radiation therapy. J Med Imaging Radiat Oncol 2018;62:81–90. https://doi.org/10.1111/1754-9485.12693.

[35] Knudtsen IS, van Elmpt W, Ollers M, Malinen E. Impact of PET reconstruction algorithm and threshold on dose painting of non-small cell lung cancer. Radiother Oncol 2014;113:210–4. https://doi.org/10.1016/j.radonc.2014.09.012.